

# Chapter 1

## Introduction

### 1.1 The Interstellar Medium

This thesis deals with observations of polarized light from galactic objects. Thus a brief introduction to the interstellar medium (ISM) should be made at this point. A thorough review of the ISM is beyond the scope of this introduction and we shall only explain in any depth those objects, regions, or entities which are relevant to an understanding of this thesis.

Observations of other galaxies, as well as our own, indicate that about 5 to 10 percent of the total mass of the galaxy is contained in the interstellar medium (ISM). The constituents of the ISM include cosmic rays, atoms, ions, molecules, and dust particles. These form the building blocks for very large objects like molecular clouds, HII regions, and supernova remnants. Each of these objects is revealed and studied in a variety of ways and wavelengths, revealing them to be quite varied in type, scale, and phase. Temperatures range from very cold ( $\sim 10 - 100$  K), dense material in molecular clouds, to very hot ( $\sim 10^6$  K), tenuous gas found in supernova remnants. The ISM is not static either but rather dynamic and a means of describing the ISM is no simple task. Perhaps the best model underlying most correct assumptions about the ISM put forth so far is by McKee and Ostriker (1977).

In the McKee-Ostriker model the ISM is distributed in four phases: 1) the Hot Ionized Medium which is found in the hot, low density cavities of supernova remnants, 2) the Warm Ionized Medium which consists of partially ionized cloud envelopes, 3) the Warm Neutral Medium which consists of the warm, neutral cloud envelopes, and 4) the Cold Neutral Medium which is found in cold cloud cores. The McKee-Ostriker model is one where the ISM is dominated by supernova remnants and each of the phases listed above is associated with a particular object. For instance, the temperature of material in the dense cores of molecular clouds is found to be quite cold, usually on the order of 100 K. These dense cores are shielded from the interstellar radiation field by the outer layers of the molecular cloud. However, the interstellar radiation field can penetrate the outer layer of the molecular cloud, thus heating it. This raises the outer layer of the cloud to higher temperature than the core, typically around  $\sim 8000\text{K}$ . This warmer outer layer exists in pressure equilibrium with the inner cold core. These are the warm neutral medium and cold neutral medium in the McKee-Ostriker model. The warm ionized medium is the partially ionized outer layer of the cloud at a temperature of around  $\sim 8000\text{K}$ . Finally, in the McKee-Ostriker model, supernovae play a key role in the overall structure of the interstellar medium, particularly its morphology. Given their enormous energy output, supernovae are capable of drastically altering the distribution of the surrounding material. In particular, as these objects evolve, part of the large amount of energy released goes into evacuating the material surrounding it. This leaves behind a bubble of tenuous gas at a very high temperature, typically on the order of millions of degree Kelvin. The interiors of these bubbles are the hot ionized medium of the McKee-Ostriker model.

While this model has its drawbacks, (and its successes), it nonetheless provides a framework from which to understand the distribution of matter in different phases in the ISM. The McKee-Ostriker model, thus, goes a long way in describing the overall structure of the ISM; however, other theories exist to explain the nature of the objects which exist in the ISM. The most noticeable among these are HII regions. These bright glowing gas clouds are the result of stellar nurseries where newborn, hot O and B-type stars emit enough ultraviolet radiation to ionize the surrounding gas causing it to fluoresce by recombination line emission. Also important to this thesis are the supernova remnants (SNRs) that were previously discussed. In particular, SNRs which have evolved over long periods of time into large shell-like structures are of interest. The small

particles of dust are important to an understanding of the nature of the observed polarization of light associated with these regions above. Finally, running throughout the Galaxy is magnetic field. This field plays an important role in the alignment of non-spherical dust grains which is important in understanding the polarization of starlight by the ISM.

### 1.1.1 HII Regions

HII regions are among the most easily seen and spectacular objects in the Galaxy. As sites of active star formation, these objects are usually found in the spiral arms and are intimately related to molecular clouds, often appearing as blisters on molecular clouds. They achieve their luminescence in the following manner. The O and early B-type stars which formed from the material in the molecular cloud and have reached the zero age main sequence are hot enough to emit copious amounts of ultraviolet radiation. If these photons have energies greater than 13.6 eV ( $\lambda < 912 \text{ \AA}$ ) then they are capable of ionizing the surrounding hydrogen. A free electron will eventually find an  $\text{H}^+$  ion and recombine. In the process of recombination, photons are liberated as the electron cascades down to the ground state of hydrogen. Some of these photons will wind up leaving the nebula which accounts for the optical appearance. At high principle quantum number levels (high  $n$  levels) the nebula will appear bright in the radio region of the spectrum, and low  $n$  levels (particularly the Balmer series) are responsible for the nebula's optical appearance.

HII regions can be quite large. O stars can typically ionize a region hundreds of parsecs in diameter whereas B stars can only ionize a region on the order of a few parsecs. Typically a group of O and early B-type stars will form from a molecular cloud at the same time. Through their combined luminosities, this group, called an OB association, is capable of ionizing a much larger region of surrounding hydrogen. Typical number densities in the bright parts of HII regions are on the order of  $10$  to  $10^2 \text{ cm}^{-3}$ . The overall masses of HII regions are on the order of  $10^2$  to  $10^4 M_{\odot}$  ( $1M_{\odot} = 1.989 \times 10^{33} \text{ g}$ ). The abundance of elements in these nebulae is cosmic. That is, about 75% is hydrogen, 25% is helium, and 1% heavy elements.

The size of an HII region can be determined by the number of ionizing photons available from the OB association and the number density of hydrogen

atoms in the cloud. What follows is a review of the derivation of the size of an HII region presented by Osterbrock (1989). Consider to a first approximation a nebula of pure hydrogen surrounding a single hot star. At any point in the nebula the ionization equilibrium is fixed by the balance between photoionization and recombination. The equation which expresses this ionization equilibrium is

$$N_{HI} \int_{\nu_o}^{\infty} \frac{4\pi J_\nu}{h\nu} a_\nu(HI) d\nu = N_e N_p \alpha_A(HI, T) \quad (1.1)$$

where  $N_{HI}$  is the number density of neutral hydrogen,  $N_e$  and  $N_p$  are the number densities of electrons and protons respectively,  $J_\nu$  is the mean intensity of the radiation at a point in the nebula,  $h\nu$  the energy of a photon,  $\nu_o$  is the threshold frequency needed for ionization of hydrogen from the ground state,  $a_\nu(HI)$  is the ionization cross section for hydrogen, and  $\alpha_A(HI, T)$  is the total recombination coefficient in units of  $\text{cm}^3 \text{s}^{-1}$  summed over captures to all levels,

$$\alpha_A = \sum_{n,l} \alpha_{n,l}(HI, T) \quad (1.2)$$

where  $\alpha_{n,l}(HI, T)$  is the recombination coefficient to all levels with principle quantum number  $n$  and angular momentum quantum number  $l$ .

Now the radiation at any point in the nebula is the sum of the radiation from the star plus emission from the diffuse gas. If a recombination occurs directly to the ground state, then the emitted photon from the diffuse gas will have an energy capable of ionizing the surrounding hydrogen as well. For an optically thick nebula, a good approximation is that this photon will ionize another hydrogen atom in the nebula. Therefore, no ionizing photons will escape the nebula. This is called the "on-the-spot" approximation and is a good approximation since the diffuse radiation field will have a Maxwellian distribution which is strongly peaked about the ionization energy. So we may think of this process in the following way: photons from the star cause ionizations which are balanced by recombinations to excited levels, while recombinations to the ground state of hydrogen produces photons that are absorbed elsewhere in the nebula.

Now the mean intensity in equation (1.1) is simply the luminosity of the star reduced by  $1/4\pi r^2$ , as well as extinction, or  $4\pi J_\nu = L_\nu/4\pi r^2 = F_\nu(R^2/r^2)e^{-\tau}$

where  $F_\nu$  is the flux at the surface of the star and  $r$  is the distance to some point in the nebula, and  $e^{-\tau}$  represents an extinction with optical depth  $d\tau = N_{HI} a_\nu dr$ . Therefore, we may rewrite equation (1.1) in terms of the stellar flux as

$$\frac{R^2}{r^2} \int_{\nu_0}^{\infty} \frac{F_\nu}{h\nu} \frac{d\tau}{dr} e^{-\tau} d\nu = N_e N_p \alpha_A(HI, T) \quad (1.3)$$

and upon integrating over  $r$  we get

$$R^2 \int_0^\infty \int_{\nu_0}^{\infty} \frac{F_\nu}{h\nu} e^{-\tau} d\nu d\tau = R^2 \int_{\nu_0}^{\infty} \frac{F_\nu}{h\nu} d\nu = \int_0^\infty N_e N_p \alpha_A(HI, T) r^2 dr \quad (1.4)$$

Now in the ionized region, under the assumption that the nebula is pure hydrogen,  $N_e = N_p \sim N_{HI}$  and outside the ionized region  $N_e = N_p \sim 0$ . If we demarcate the boundary between the ionized region and the neutral hydrogen region by  $r_s$ , the integral on the right hand side of equation (1.4) simply becomes  $N_{HI}^2 \alpha_A(HI, T) r_s^3/3$ . The second integral in equation (1.4) can be written in terms of the stellar luminosity since  $L_\nu = 4\pi R^2 F_\nu$  at the surface of the star. Therefore, we may write (1.4) as

$$\int_{\nu_0}^{\infty} \frac{L_\nu}{h\nu} d\nu = \frac{4\pi}{3} N_{HI}^2 \alpha_A(HI, T) r_s^3 \quad (1.5)$$

or, by noting that the integral in this equation is simply the total number of ionizing photons emitted per second from the star and denoting this by  $Q^*$ , we have as the expression for the radius of the ionized region

$$r_s = \left[ \frac{3}{4\pi} \frac{Q^*}{\alpha_A(HI, T)} \right]^{1/3} N_{HI}^{-2/3} \quad (1.6)$$

The radius derived in the equation above is usually referred to as the Strömngren radius, named after B. Strömngren who first derived the result in 1939. The sphere of ionized hydrogen is called a Strömngren sphere. While this result was derived for a nebula of pure hydrogen it nonetheless yields a good first order approximation for the radius of nebula whose central star is capable of producing ionizing radiation. While actual nebula will contain a mixture of both hydrogen and helium, Osterbrock (1989) has shown that for an O6 star, the region of ionization of hydrogen and helium are coincident, and a cooler B0 star will have a region of ionized hydrogen larger than a region of ionized helium.

Nebulae which contain even heavier elements will have an even smaller region of ionized heavy elements than either the hydrogen or helium regions.

While there is not only heating of the gas that goes on by the stellar UV radiation, there are also mechanisms which cool the gas. Cooling of the nebula occurs when photons are produced that no longer produce any further ionization of the H or He. These photons will then escape the nebula since they are no longer capable of adding to the overall energy input into the nebula. There are three main mechanisms which contribute to the cooling: 1) recombination of hydrogen and helium to states other than the ground state, 2) collisional excitation of ions such as  $O^+$ ,  $O^{++}$ , and  $N^+$  and subsequent emission, and 3) free-free (or Bremsstrahlung) transitions. The most effective of these three mechanisms is the collisional excitation of the ion species mentioned. Even though these species are not in abundance, they are nevertheless better at cooling than collisional excitation of hydrogen or helium since they have energy levels with excitation energies of only a few  $kT$  above the ground state. Therefore, collisions of these ions with thermal electrons excite the electrons to these states where forbidden transitions occur with an emission rate of about  $4 \times 10^{-5} s^{-1}$ . Since these emitted lines have too low an energy to excite any further atoms in the gas, they escape the nebula, thus effectively cooling it.

While the cooling of these HII regions occurs most effectively by the collisional process, they nonetheless remain quite high in temperature. The temperature of a typical HII region is on the order of  $10^4$  K and will remain this high for as long as the exciting stars continue on the main sequence. However, once these exciting stars move off the main sequence, they are no longer able to produce large quantities of UV radiation. This effectively shuts off the nebula's ionizing photons. With no further input from the stellar sources, the HII region will still have a diffuse radiation field produced by the on-the-spot ionizations. However, eventually these too will cease to be numerous and the nebula will eventually start to fade. This fossil HII region will eventually fade out.

From the above discussion it should be clear that HII regions emit at many different wavelengths corresponding to atomic transitions of hydrogen, helium, and other heavy element species. Calculations of the relative line strengths of H and He relative to  $H\beta$  by Osterbrock (1989) show that the Balmer alpha or  $H\alpha$  line is the strongest optical line which leaves the nebula. Not only are there line emissions but also a continuum emission as well. This continuum emission is

weak in the optical, resulting from free-bound transitions and two photon decay of the  $2s^0$  state ( i.e.  $2s^0 \rightarrow 1s^0$  requires 2-photon emission ) which are stronger than the free-free transitions. However, in the radio and infrared, free-free transitions are much stronger.

In the discussion so far we have assumed that the HII region is static. However, this will not be the case since the photoionization can not take place everywhere within the Strömgren radius instantaneously. After a hot star has reached the main sequence and is producing UV photons at a constant rate, ionization takes place in the immediate vicinity of the star. This will increase the temperature by a factor of  $\sim 100$  and the number density of gas particles by a factor of two. Therefore, the pressure in the ionized region is about 200 times greater than in the surrounding neutral medium. Thus, the ionized gas will expand into the neutral region. A boundary, or front, will exist between the ionized and neutral gas which propagates outward. This front is commonly referred to as an ionization front. Dyson and Williams (1980) derived the velocity of the ionization front as it relates to its distance from the star and the Lyman continuum output of the star. I shall present a summary of their derivation which describes the evolution of the ionization front.

Assume that the gas surrounding the star is initially at rest in the frame of reference of the star. At some particular time  $t$ , the ionization front is at a distance  $R$  from the star. Let  $N_c$  be the number of ionizing photons falling on a unit area of the ionization front per second and  $N_{HI}$  be the density of the neutral gas. Since the gas behind the ionization front is assumed to be fully ionized and neutral in front of it, then, assuming ionization equilibrium, when the front has moved a distance  $dR$ , then enough ionizing photons have had to reach the front in order to ionize the material just behind the front. That is,  $N_c dt$  photons are needed to ionize  $N_{HI} dR$  amount of gas, or  $N_c dt = N_{HI} dR$ . Therefore, the ionization front velocity is  $dR/dt = N_c/N_{HI}$ . Now, since the ionization front is actually spherical, there will exist a geometrical dilution factor. Likewise, inside the nebula, recombinations continually take place creating neutral atoms. By assuming that the rate at which UV photons are produced by the star equals the rate at which they arrive at the ionization front plus, the rate at which they are absorbed by the neutral gas in the ionized region, we can say that

$$Q^* = 4\pi R^2 N_c + \frac{4\pi}{3} R^3 N_{HI}^2 \alpha_A(HI, T) \quad (1.7)$$

then, the velocity of the ionization front is

$$\frac{dR}{dt} = \frac{N_c}{N_{HI}} = \frac{Q^*}{4\pi R^2 N_{HI}} - \frac{1}{3} R N_{HI} \alpha_A(HI, T) \quad (1.8)$$

As can be seen by equation (1.8) the ionization front will decrease in velocity as time increases, but expansion continues as long as the gas pressure in the ionized region is high. Simple models by Dyson and Williams (1980) show that unless the surrounding gas density is quite high, a pressure equilibrium will not be reached.

Besides the mechanism stated above, the evolution of these regions are also determined by strong stellar winds and supernovae. O and early B type stars have strong stellar winds as well as prodigious mass loss rates compared to other stars. Typical stellar winds are on the order of  $2000 \text{ km s}^{-1}$  and mass loss rates on the order of  $10^{-6} M_{\odot} \text{ yr}^{-1}$ . While these were not considered in the discussion of HII regions above, we shall give a quick review of their effect on the surrounding interstellar gas. If the initial main sequence mass of the star is  $> 8 M_{\odot}$  then the final stage of stellar evolution for the star is a supernova. These shall be discussed in the next section.

### 1.1.2 Shells and Supernova Remnants

The evolution of HII regions is not just confined to the propagation of an ionization front as discussed above. Observations have shown that O and early B-type stars have strong stellar winds. The mechanical energy per year imparted to the ISM is  $\dot{E}_s = \frac{1}{2} \dot{M} v^2 \sim 10^{42} \text{ erg yr}^{-1} \sim 8 L_{\odot}$  (where  $L_{\odot}$  is the Sun's luminosity,  $1.2 \times 10^{41} \text{ erg yr}^{-1}$ ), and over the typical lifetime of such stars can impart  $\sim 10^{49}$  ergs into the ISM. Such a large amount of energy going into the ISM can sweep up the gas in the vicinity around the star, creating a shell of neutral material surrounding it. Models determining the structure and dynamics of these wind driven shells have been put forth by Castor et al. (1975), Weaver et al. (1977), and Bruhweiler et al. (1980), each dealing with particular phases of evolution. Most everyone agrees there will be four phases of evolution of a wind blown shell. The initial phase is one of free expansion which lasts for only a short time, typically on the order of a few centuries. This will be followed by a phase of adiabatic expansion lasting a few thousand years. The next stage is

usually referred to as the "snowplow" phase since the interstellar matter is pushed into a thin cold shell. Finally, the shell will dissipate into the surrounding medium. The longest stage of evolution is the snowplow phase. A simple model based on the ones presented by Dyson and Williams (1980) which describe the snowplow phase is presented below.

Consider an O or early B-type star surrounded by an HII region. After the first two stages of evolution, the bubble enters the snowplow phase. Let us suppose a thin shell of neutral hydrogen has been swept-up into a thin shell surrounding the star. We consider the shell thickness to be smaller than the radius of the swept out region ( $\Delta R \ll R$ ) so that  $R$  will be the variable which describes the shell. We also consider that the interior of the shell is filled with the hot, shocked wind which exerts a uniform pressure  $P$  on the shell. The equation of motion for the shell is then

$$\frac{d}{dt} \left( \frac{4\pi}{3} R^3 n_o m_H \dot{R} \right) = 4\pi R^2 P \quad (1.9)$$

where  $n_o$  is the number density of hydrogen before the material was swept-up into a shell,  $m_H$  is the mass of hydrogen, and  $\dot{R}$  is the velocity of the shell. Differentiating equation (1.9) leads to

$$P = \frac{n_o m_H}{3} \left( 3 \dot{R}^2 + R \ddot{R} \right) \quad (1.10)$$

Now the stellar wind adds energy to the region just behind the shell at a rate of  $\dot{E}_s$ . Energy in this region is lost by the work done on the shell. Therefore, in the region just behind the shell, the conservation of energy equation is

$$\frac{d}{dt} \left( \frac{4\pi}{3} R^3 \frac{3}{2} P \right) = \dot{E}_s - P \frac{d}{dt} \left( \frac{4\pi}{3} R^3 \right) \quad (1.11)$$

where the left hand side represents the rate of change of thermal energy using the fact that the internal energy for a monatomic gas is 3/2 times the pressure, and the second term on the right hand side is the rate at which the hot gas does work on the neutral hydrogen. Differentiation of this equation leads to

$$5 \dot{R} P + R \dot{P} = \frac{\dot{E}_s}{2\pi} \quad (1.12)$$

Upon combining equations (1.10) and (1.12) we get

$$R^4 \ddot{R} + 12R^3 \dot{R} \ddot{R} + 15R^2 \dot{R}^3 = \frac{3}{2\pi} \frac{\dot{E}_s}{n_o m_H} \quad (1.13)$$

which is an equation describing the radial evolution of the shell of swept-up material. The solution of this equation is

$$R(t) = \left( \frac{125}{154\pi} \right)^{1/5} \left( \frac{\dot{E}_s t^3}{n_o m_H} \right)^{1/5} \quad (1.14)$$

which describes the radial evolution of the shell as a function of ambient gas density, stellar mass loss  $\dot{E}_s$ , and time. Considering  $\dot{E}_s = 10^{42} \text{ergs yr}^{-1}$  and taking  $n_o = 10^2 \text{cm}^{-3}$ , over the lifetime of the star this leads to a shell whose radius is on the order of a few parsecs.

The simple model presented above is unrealistic since most HII regions surround OB associations and not single stars. This means that the combined stellar energy outputs need to be considered. This will increase the size of the shell since the energy input term  $\dot{E}_s$  will be much higher. An example of a shell which is believed to have evolved in the manner just described is the Rosette Nebula. This HII region in Monoceros has a central cavity that is about 7 pc in diameter and is powered by O and B-type stars at the center of the nebula.

While the above analysis considered only the snowplow phase of the shell's evolution, we should also consider what the final evolution of the shell will be when the more massive stars which power it leave the main sequence. If the initial mass of the star is greater than eight solar masses, the end point of stellar evolution for a star is as a supernova which typically liberates energy on the order of  $10^{51} \text{ergs}$ . The evolution of the shell when the combined energy release for a group of stars that go supernova has been studied analytically by Bruhweiler, et al. (1980), Cox, D.P., (1972) and McCray and Kafatos (1987) as well as numerically by Tomisaka, et al. (1980, 1986), Mineshige, et al. (1993), MacLow, et al. (1989), Igumentshchev, I.V., et al. (1990), and Tenorio-Tagle, et al. (1987). While we shall not derive any formulae which model the evolution of these supershells, we will state that typical sizes of these objects is on the order of hundreds of parsecs. Evolution of these shells have been carried to the extreme by even considering the possibility that these objects become so large compared to the scale height of the galaxy that they suffer Rayleigh-Taylor instability and "burst" through to the galactic halo. Any matter inside the shell

that would be able to reach the halo by the action of the stellar winds in the shell would become what some call a "galactic chimney", a term first coined by Norman and Ikeuchi (1989).

While most of the authors above have neglected the magnetic field associated with these objects, a few have incorporated the magnetic pressure in their models. The magnetic pressure is important in determining whether or not the shell will actually break through the galactic disk or not. The existence of this magnetic pressure is due to the fact that the magnetic field becomes entrained in the gas when it is ionized. As the shell expands, the magnetic field becomes compressed and distorted, exerting a pressure  $B^2/4\pi$  on the shell. Therefore, means of detecting and measuring the magnetic field associated with these shells would be useful in calculating the magnetic pressure associated with these objects.

While there are ways of detecting this magnetic field in the radio, by Zeeman splitting of hydrogen in the shell, for example, a method of optical detection may be possible as well. Since shells, both wind and supernova driven, contain O and B-type stars within them, there is the likelihood that the UV radiation from these stars will ionize the inner walls of these shells, thus producing recombination lines which can be detected. It is just such a mechanism that is believed to be at work in the shell associated with the W4 star forming region imaged in the Balmer alpha line by Dennison et al. (1995). By imaging the  $H\alpha$  line through polarimetry, it may be possible to detect polarization due to aligned dust grains along the magnetic field associated with the shell. In the case of HII regions, the shell-like structure of the Rosette Nebula makes it a prime candidate for such a study.

### 1.1.3 Dust

The average number density of atoms in the ISM is about 0.1 per cubic centimeter, where, naturally, regions of higher and lower density exists. While this may seem like a trivial amount of material, the mass of the ISM is on the order of several billion solar masses, i.e. about 1% the mass of the galaxy. About 1% of the total mass of the ISM is locked up in submicron size particles of heavier atoms and molecules which are generally referred to as dust particles.

While most of the ISM is cosmic in abundance, these heavier elements have been forged in the furnaces of stellar formation.

Whereas observations of stars and glowing HII regions are easily made, direct evidence of dust is harder to obtain. The effect of interstellar dust on starlight is three fold; extinction, reddening, and polarization. Extinction occurs because starlight is absorbed or scattered by dust, thus making a star appear dimmer than it actually is. Reddening occurs because blue light is scattered more effectively than red, hence the term reddening. Finally, polarization results from the selective extinction of aspherical aligned dust grain aligned with the galactic magnetic field. Dust is also revealed by the scattering of starlight from such objects as reflection nebulae. Observations of dust have been made at many wavelengths.

Observations in the millimeter wavelength range have revealed that dust particle have an emissivity proportional to  $\nu^\beta$ , where  $\beta$  is a constant. Millimeter, as well as infrared observations reveal information about the emissivity of dust grains. In particular, infrared observations have provided information about the emissivity efficiency as a function of wavelength, as well as grain composition by the study of emissivity-wavelength curves. Infrared observations yield information on grain sizes as well. Optical observations provide information on the extinction, scattering, and polarization properties of dust, as mentioned above. The wavelength dependence of extinction provides information about the sizes of particles. Extinction properties of dust are also provided by ultraviolet observations. However, UV observations provide information only about objects which are relatively nearby. Given that the number density of hydrogen in the ISM is about  $0.1 \text{ cm}^{-3}$  and has an ionization cross section of  $3 \times 10^{-27} \text{ cm}^2$ , the mean free path through the ISM is  $\sim 0.1$  parsec before a UV photon with wavelength  $< 912 \text{ \AA}$  ionizes a hydrogen atom. Shortward of  $100 \text{ \AA}$ , the ISM becomes transparent to soft x-rays, allowing studies of scattering of x-ray radiation to be made.

While observations of the large scale distribution of dust reveal its presence to be widespread, it is mostly contained in the spiral arms of the galaxy and mostly associated with population I stars. Studies have shown that dust grains are associated strongly with the galactic disk in a layer about  $\sim 200$  parsec thick in the solar neighborhood with the gas and dust well mixed. Small scale observations of the distribution of dust in the ISM reveal that it is extremely

clumpy. Generally a correlation exists between extinction by dust and distance in the galactic plane. Observations of stars that are a few kiloparsecs from the Sun have shown empirically that the ratio of the average amount of total extinction to distance is about 1 magnitude per kiloparsec.

Studies of the emissivity and extinction of dust show that grains have sizes typically ranging from a few nanometers to around 1 micrometer. The definitive composition of these grains is an ongoing question. While observations of scattering and extinction reveal information about the dimensional parameters of grains, only spectroscopy reveals any information about the chemical composition of grains. Many models of grain composition have been put forth to match observations of extinction ranging from ice covered silicates, to refractory minerals, to biological organisms such as bacteria.

Whereas the composition of grains is an unanswered question, the origins of dust grains seem to be well established, particularly since there exists a strong correlation between dust and stars. Dust is generally believed to originate in the "cool" outer layers of evolved stars such as red giants, supergiants, and AGB (Asymptotic Giant Branch) stars. The outer atmospheres of these stars are cool enough and have high enough densities to be sites of grain nucleation. Dust grains in the ISM can be explained by their entrainment in the winds associated with these stars. Eventually, this dust material mixes with the material in the ISM, eventually ending up in molecular clouds. Star formation in the molecular cloud can be stimulated by supernovae shock waves which can compress regions of the molecular cloud causing condensations and star formation to occur. Thus, grains are associated with star formation and such objects as circumstellar shells and HII regions. As such, we should be able to detect the presence of dust by scattering, extinction, and perhaps even polarization around these stars and, in particular, around sites of new star formation such as HII regions.

## 1.2 Polarization

The nature of light is that it can be thought of as a wave or particle, and an appropriate view depends on the type of experiment or phenomenon under scrutiny. For example, the particle nature of light is needed in order to explain the photoelectric effect, whereas diffraction is best understood if light is thought

of as a wave. It is this latter view of light that we shall find useful in explaining the observations presented in this thesis, particularly, the polarization state of light from a stellar or galactic source.

In order to describe the polarization state of light, we shall find Stoke's vectors very useful. These are four intensity parameters which wholly describe the polarization state of light. Three of the four parameters which describe linearly polarized light are obtained by a simple means of intensity measurements made using an optical device which detects linear polarization, such as a piece of Polaroid. In the next section we shall derive these three of the four parameters and explain the basic method of observation needed to obtain them.

We will also introduce the methods by which light from galactic sources is polarized. We shall pay particular attention to scattering since it plays a central role in the analysis of chapter four, but we will also describe the method of polarization by selective extinction by aligned interstellar dust grains. This will be particularly useful since starlight can be polarized in this manner. In Chapter 3 we present measurements of starlight that has been polarized by this mechanism.

### 1.2.1 Stoke's Parameters

Since light can be thought of as transverse electromagnetic wave, we need an equation which represents the wave. The basic equation which describes the electric field vector of an electromagnetic wave in rectangular coordinates which is propagating in the  $\hat{\mathbf{k}}$  direction at some time  $t$  is

$$\mathbf{E}(\mathbf{x}, t) = (\hat{\mathbf{e}}_1 E_1 + \hat{\mathbf{e}}_2 E_2) e^{i\hat{\mathbf{k}} \cdot \mathbf{x} - i\omega t} \quad (1.15)$$

where  $\hat{\mathbf{e}}_1$  and  $\hat{\mathbf{e}}_2$  are unit vectors along Cartesian coordinates axes,  $E_1$  and  $E_2$  are complex numbers representing the amplitude, and  $\omega$  is the angular frequency of the wave. Equation (1.15) is the sum of two linearly independent electromagnetic waves which have polarizations along the  $\hat{\mathbf{e}}_1$  axis and  $\hat{\mathbf{e}}_2$  axis. Thus equation (1.15) represents the most general homogenous plane wave propagating in the  $\hat{\mathbf{k}}$  direction. The reason the amplitudes  $E_1$  and  $E_2$  are

complex numbers is to allow for the possibility of a phase difference between the two waves of different polarization. For example, if  $E_1$  and  $E_2$  have different, unequal phases, then the wave is said to be elliptically polarized. If they were to have the same magnitude, (i.e.  $E_1 = E_2$ ), then the wave is circularly polarized and described by the equation

$$\mathbf{E}(\mathbf{x}, t) = E_o(\widehat{\mathbf{e}}_1 \pm i\widehat{\mathbf{e}}_2) e^{i\widehat{\mathbf{k}} \cdot \mathbf{x} - i\omega t} \quad (1.16)$$

where  $i = \sqrt{-1}$  and the choice of sign is used to indicate whether the wave is right circularly polarized (+) or left circularly polarized (-). If, however, the amplitudes  $E_1$  and  $E_2$  have the same phase, then the wave is said to be linearly polarized. This wave will then have a magnitude  $E = [E_1^2 + E_2^2]^{1/2}$  and make an angle  $\theta = \tan^{-1}(E_2/E_1)$  with respect to the  $\widehat{\mathbf{e}}_1$  axis.

Since we are concerned with describing the magnetic field with selected regions in the galaxy, we find that observations of the linear polarization of light are well suited for this task since observations indicate that circular polarization is weak. Therefore, we need a method which can completely describe the linear polarization of the electric vector of an electromagnetic wave. This method is found via the Stoke's parameter which are defined below by Jackson (1975) as

$$I = |\widehat{\mathbf{e}}_1 \cdot \mathbf{E}|^2 + |\widehat{\mathbf{e}}_2 \cdot \mathbf{E}|^2 = A_1^2 + A_2^2 \quad (1.17a)$$

$$Q = |\widehat{\mathbf{e}}_1 \cdot \mathbf{E}|^2 - |\widehat{\mathbf{e}}_2 \cdot \mathbf{E}|^2 = A_1^2 - A_2^2 \quad (1.17b)$$

$$U = 2 \operatorname{Re} [(\widehat{\mathbf{e}}_1 \cdot \mathbf{E})^*(\widehat{\mathbf{e}}_2 \cdot \mathbf{E})] = 2A_1A_2 \cos(\delta_1 - \delta_2) \quad (1.17c)$$

$$V = 2 \operatorname{Im} [(\widehat{\mathbf{e}}_1 \cdot \mathbf{E})^*(\widehat{\mathbf{e}}_2 \cdot \mathbf{E})] = 2A_1A_2 \sin(\delta_1 - \delta_2) \quad (1.17d)$$

where the complex amplitudes have been written as a scalar multiplied by a complex phase factor, (i.e.,  $E_1 = A_1 e^{i\delta_1}$ ,  $E_2 = A_2 e^{i\delta_2}$ ). Each of the four parameters ( $I$ ,  $Q$ ,  $U$ ,  $V$ ) have units of intensity and represents the tendency of light to be in a particular state of polarization; the parameter  $I$  measures the total intensity of the light,  $Q$  the tendency for polarization along the  $\widehat{\mathbf{e}}_1$  axis over the  $\widehat{\mathbf{e}}_2$  axis,  $U$  the preference for polarization along an axis at  $+45^\circ$  (with respect to  $\widehat{\mathbf{e}}_1$ ) over polarization along an axis at  $135^\circ$  (with respect to the  $\widehat{\mathbf{e}}_1$  axis), and  $V$  the tendency for light to be circularly polarized. If the light ray is completely (or partially) linearly polarized, then  $V$  is zero and the ray is described by  $I$ ,  $Q$ , and

$U$ . If the light is unpolarized then only  $I$  will remain. We can see that these four parameters are not independent and obey the relationship

$$I^2 = Q^2 + U^2 + V^2 \quad (1.18)$$

which is easily derived from equations (1.17a...d) above.

While equations (1.17a...d) are the definitions of the Stoke's parameter, these expressions are not particularly well suited for the actual measurement of light. Since any quantity can not be measured at an exact instant of time but rather over some finite time interval, the observed Stoke's parameters are in reality time averaged intensities. However, in order to simplify the notation in this section we shall leave off any time averaging symbols, instead electing to remember that time averages are involved. Furthermore, it would be nice to have a means of relating an actual optical device which detects polarization to the Stoke's parameters. One of the nice properties of the Stoke's parameters is that this requirement is realizable. That is, equations (1.17a...d) can be written in terms of observed intensities as

$$I = I_0 + I_{90} \quad (1.19a)$$

$$Q = I_0 - I_{90} \quad (1.19b)$$

$$U = I_{45} - I_{135} \quad (1.19c)$$

$$V = I_{rcp} - I_{lcp} \quad (1.19d)$$

where  $I_\theta$  is the intensity of light measured by a linear polarizer oriented at an angle  $\theta$  with respect to some fiducial setting and  $I_{rcp}$  and  $I_{lcp}$  are the right and left circular polarized intensities. Therefore, to measure the linear polarization state of a polarized (or partially polarized) source of light, we simply need to make four intensity measurements with a linear polarizer oriented at four different angles, say  $0^\circ$ ,  $45^\circ$ ,  $90^\circ$ , and  $135^\circ$ , and, use simple arithmetic to determine  $I$ ,  $Q$ , and  $U$ .

Another nice property of the Stoke's parameters is that  $I$ ,  $Q$ ,  $U$ , and  $V$  are additive for individual waves. However, for natural light, amplitude ratios  $A_1^2/A_2^2$  and phase differences  $\delta_1 - \delta_2$  are not correlated and so by the additive property, the resulting sums of individual values of  $Q$ ,  $U$ , and  $V$  are each zero.

However, if a correlation does exist, a partial polarization will be observed. Knowing this we can write the Stoke's parameters in two parts: a non-polarized part denoted by  $I_1$ ,  $Q_1 = U_1 = V_1 = 0$ , and a completely polarized part denoted by  $I_2$ ,  $Q_2$ ,  $U_2$ ,  $V_2$ . Using these, the degree of linear polarization  $p$  can be written as

$$p = \frac{\sqrt{Q_1^2 + Q_2^2 + U_1^2 + U_2^2}}{I_1 + I_2} = \frac{\sqrt{Q_2^2 + U_2^2}}{I} \quad (1.20)$$

where  $I = I_1 + I_2$ . Likewise, the angle the electric vector makes with respect to a fiducial setting is

$$\theta = \frac{1}{2} \tan^{-1} \frac{U_2}{Q_2} \quad (1.21)$$

(Since  $Q_1 = U_1 = 0$ , we shall drop the subscripts on  $Q_2$  and  $U_2$ ). It is useful to write the Stoke's parameters  $Q$  and  $U$  normalized with respect to the total intensity  $I$  as  $Q/I = q$  and  $U/I = u$ . Using this notation the degree of linear polarization and the position angle of the electric vector becomes

$$p = \sqrt{q^2 + u^2} \quad (1.22)$$

$$\theta = \frac{1}{2} \tan^{-1} \frac{u}{q} \quad (1.23)$$

Since equations (1.19a..c) are particularly important in this thesis for the measurement of linear polarization of light, we shall derive these expression. We can see that equation (1.17a) and (1.17b) readily lend themselves to equations (1.19a) and (1.19b) respectively since the intensity is proportional to the square of the amplitude of the electric vector,  $I \propto E^*E$ . That is, using the fact that  $E_1$  and  $E_2$  can be written as a real part with a complex phase,  $I_0 = A_1 e^{i\delta_1} A_1 e^{-i\delta_1} = A_1^2$  and  $I_{90} = A_2^2$ . Therefore, it is easily seen that  $I = A_1^2 + A_2^2 = I_0 + I_{90}$  and that  $Q = A_1^2 - A_2^2 = I_0 - I_{90}$ .

In order to derive equation (1.19c) from (1.17c), we first write equation (1.15) in the Cartesian coordinate system with basis vectors  $\pm 45^\circ$  with respect to the  $\hat{e}_1$  and  $\hat{e}_2$  axes. This is a proper transformation since any linearly polarized wave can be thought of as having two mutually orthogonal polarization vectors. Since we are taking the complex conjugate of the

quantities of interest, we can neglect the  $\exp(i\hat{\mathbf{k}} \cdot \mathbf{x} - i\omega t)$  term since the product of this quantity with its complex conjugate is unity. Letting  $\hat{\mathbf{e}}_{45}$  and  $\hat{\mathbf{e}}_{135}$  represent the unit vectors of a coordinate system rotated  $45^\circ$  with respect to the  $\hat{\mathbf{e}}_1$  axis, the electric vector (1.15) can be written in terms of these coordinates by a rotation through  $45^\circ$  as

$$\begin{pmatrix} E_{45} \\ E_{135} \end{pmatrix} = \begin{pmatrix} \cos \theta & \sin \theta \\ -\sin \theta & \cos \theta \end{pmatrix} \begin{pmatrix} E_1 \\ E_2 \end{pmatrix} = \frac{1}{\sqrt{2}} \begin{pmatrix} E_1 + E_2 \\ E_2 - E_1 \end{pmatrix} \quad (1.24)$$

where, in vector notation, the resulting rotated electric vector is

$$\mathbf{E} = \frac{1}{\sqrt{2}}(E_1 + E_2)\hat{\mathbf{e}}_{45} + \frac{1}{\sqrt{2}}(E_2 - E_1)\hat{\mathbf{e}}_{135} \quad (1.25)$$

Now the intensity of this wave is given by  $I = \mathbf{E}^* \mathbf{E}$ , or more specifically,

$$I_{45} = \frac{1}{2}(E_1 + E_2)^*(E_1 + E_2) \quad (1.26)$$

$$I_{135} = \frac{1}{2}(E_2 - E_1)^*(E_2 - E_1) \quad (1.27)$$

Using the fact that  $E_1 = A_1 e^{i\delta_1}$  and  $E_2 = A_2 e^{i\delta_2}$ , the two equations above can be rewritten as

$$I_{45} = \frac{1}{2} \left[ A_1^2 + A_2^2 + A_1 A_2 (e^{i(\delta_1 - \delta_2)} + e^{-i(\delta_1 - \delta_2)}) \right] \quad (1.28)$$

$$I_{135} = \frac{1}{2} \left[ A_1^2 + A_2^2 - A_1 A_2 (e^{i(\delta_1 - \delta_2)} + e^{-i(\delta_1 - \delta_2)}) \right] \quad (1.29)$$

Taking the difference between equations (1.28) and (1.29), we find that

$$I_{45} - I_{135} = A_1 A_2 (e^{i(\delta_1 - \delta_2)} + e^{-i(\delta_1 - \delta_2)}) = 2A_1 A_2 \cos(\delta_1 - \delta_2) \quad (1.30)$$

where we have used the fact that  $Re(e^{i\theta} + e^{-i\theta}) = \cos(\theta)$  in the above expression. We see that the right hand side of equation (1.30) is the definition of the Stoke's parameter  $U$ . Therefore, by measuring the difference in intensities with a Polaroid oriented at  $45^\circ$  and  $135^\circ$  we can easily obtain the parameter  $U$ . We now establish that equation (1.25) satisfies equation (1.17c). That is, using equation (1.25) for  $\mathbf{E}$  in equation (1.17c) we can easily show that

$U = 2A_1A_2\cos(\delta_1 - \delta_2)$ . Consider equation (1.17c) with equation (1.25) substituted for  $\mathbf{E}$

$$U = 2\text{Re} [(\hat{\mathbf{e}}_1 \cdot \mathbf{E})^*(\hat{\mathbf{e}}_2 \cdot \mathbf{E})] \quad (1.31)$$

Considering each term separately in the equation above, it can be easily shown that

$$\hat{\mathbf{e}}_1 \cdot \mathbf{E} = \hat{\mathbf{e}}_1 \cdot \frac{(E_1^* + E_2^*)}{\sqrt{2}} \hat{\mathbf{e}}_{45} + \hat{\mathbf{e}}_1 \cdot \frac{(E_2^* - E_1^*)}{\sqrt{2}} \hat{\mathbf{e}}_{135} = E_1^* \quad (1.32)$$

$$\hat{\mathbf{e}}_2 \cdot \mathbf{E} = \hat{\mathbf{e}}_2 \cdot \frac{(E_1 + E_2)}{\sqrt{2}} \hat{\mathbf{e}}_{45} + \hat{\mathbf{e}}_2 \cdot \frac{(E_2 - E_1)}{\sqrt{2}} \hat{\mathbf{e}}_{135} = E_2 \quad (1.33)$$

which, when substituted back into equation (1.31) yields

$$U = 2\text{Re} [E_1^* E_2] = 2\text{Re} [A_1 A_2 e^{-i(\delta_1 - \delta_2)}] = 2A_1 A_2 \cos(\delta_1 - \delta_2) \quad (1.34)$$

which proves equation (1.19c) using the electric vector written as equation (1.25).

We have spent some time deriving the method used to measure and describe the linear polarization of light. We have shown that the Stoke's parameters written in terms of observables (equations 1.19a...c) allows one to determine the percent polarization and position angle the electric vector makes with respect to a fiducial setting, (equations 1.20 through 1.23). We have done so since these methods lie at the heart of this thesis. That is, the linear polarization state of light from a cosmic source is measured by imaging regions of the sky with a linear polarizer oriented at  $45^\circ$  angles with respect to one of the axes of the CCD chip. These images are then combined via equations (1.19a...c) to determine the Stoke's parameters  $I$ ,  $Q$ , and  $U$ , and, from these, the degree of linear polarization and the position angle the electric vector makes with respect to one of the axes of the CCD chip. The position angle can then be related to a reference system on the celestial sphere. The particular transformation is discussed in Chapter 3.

Having introduced the Stoke's parameters and their use in measuring the state of polarization of electromagnetic wave, we next turn our attention to the methods which are responsible for producing polarization. Particularly, among these are polarization by scattering and by selective extinction.

## 1.2.2 Polarization By Scattering

Polarization by scattering is a very common occurrence because scattering is so pervasive. In fact, rarely, do we detect any source of radiation where scattering has not had at least some influence on the passage of radiation from the source to our detector. The degree to which scattering becomes important is related to the size of the scattering particle and the wavelength of radiation under study. In particular the size of the scattering cross section is of importance, not necessarily the actual physical cross section itself. The size of the particle also determines the relationship between extinction and wavelength. For instance, if the scattering agents were electrons, then the cross section is the Thomson cross section, and the extinction is nearly independent of the wavelength of light. Similarly, when the particles are large compared to the wavelength of light, the extinction is also independent of wavelength.

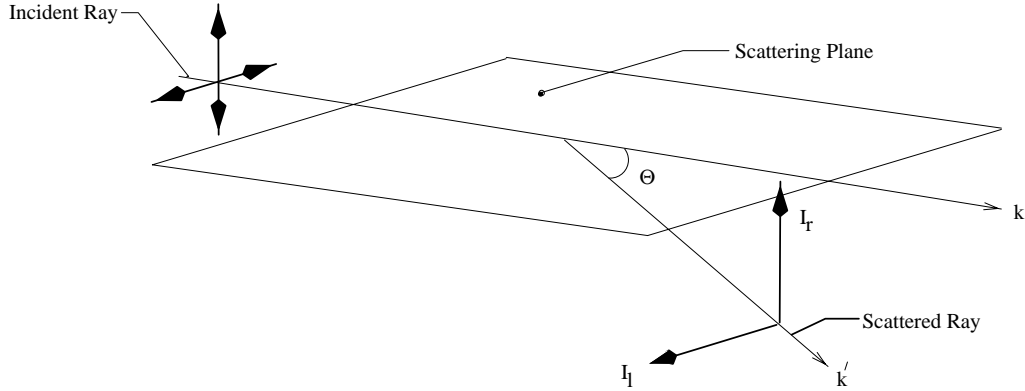
Suppose an unpolarized electromagnetic wave is propagating in the  $z$  direction in a Cartesian coordinate system. If this wave is incident upon a particle, the electric vector will set the atomic electrons into oscillation in the  $x$ - $y$  plane in response to the electric field of the incident wave. Since the wave was unpolarized, there will be no preferred direction of oscillation in the  $x$ - $y$  plane. Now, an oscillating dipole does not radiate in the direction of its motion, and so the scattered radiation will be partially polarized in the  $x$ - $y$  plane. The polarization will be zero for forward and back scattering, but will be 100% (theoretically) at  $90^\circ$  with respect to the direction of propagation. For instance, light from the sun is polarized by particles in the earth's atmosphere reaching as high as 70 to 80 percent at right angles to the direction of propagation.

Figure 1.1 shows the geometry of scattering by a small particle. The incident radiation is unpolarized, propagating in a direction  $\hat{\mathbf{k}}$ . The radiation is scattered in the  $\hat{\mathbf{k}}'$  direction which makes an angle  $\Theta$  with respect to the direction of propagation, and is partially polarized with components  $I_l$  and  $I_r$  which are at right angles to each other and the direction of propagation. The component  $I_l$  lies in the plane of scattering whereas  $I_r$  is perpendicular to it.\* It was shown by Mie (1908) that a small homogenous sphere will scatter light in just such a

---

\*The plane of scattering is considered to be the plane containing the incident and scattered ray.

manner and expressions were derived for the two scattered components  $I_l$  and  $I_r$  as a function of  $\Theta$  and the index of refraction of the scattering particle.



**Figure 1.1** Polarization by scattering from a particle. Incident unpolarized radiation propagating in direction  $k$  is scattered at an angle  $\Theta$  resulting in partial polarization with intensities  $I_l$  and  $I_r$ .

Since this thesis deals with the optical wavelengths, we shall primarily be concerned with scattering of light by dust grains. Typically, dust grains in the ISM have sizes on the order of 0.1 to 1  $\mu\text{m}$ . Since the wavelength of light detected in this thesis is 0.65  $\mu\text{m}$ , scattering by smaller particles is most likely described by Rayleigh scattering while for larger particles is better understood in terms of diffraction. The dust grains themselves have a complex refractive index of the form  $n = n' - in''$ . Dust grains are most likely to have irregular shapes, not spherical, as evidenced by polarization by selective extinction. Therefore, a complete theory, or even a quick review, of scattering models which takes all these factors into account is not possible in the limited space available. However, a model based on Rayleigh scattering is presented later in this thesis (section 4.5.2 of Chapter 4).

### 1.2.3 Polarization by Selective Extinction

As its name implies, polarization by selective extinction results from the extinction of light whose electric vector is in some preferred orientation. Suppose natural light is incident on a solid particle, a dust grain. Since natural light is unpolarized, the electromagnetic wave's electric vector has no preferred orientation as in the case of polarized, or partially polarized light. If the dust grain is spherical, then the wave will suffer extinction either by scattering or absorption of the incident light. As mentioned in the last section, the scattered light will have a partial polarization when scattered at some angle away from the propagation direction, but will not if the scattered ray propagates in the same direction as the incident ray. Also, due to the symmetry of the grain, no net orientation of the wave's electric vector will result from the scattering or absorption process, since all directions of scattering or absorption are equally likely. However, this is not the case if the grain is not spherically symmetric. Natural light incident on a non-spherical grain will suffer selective extinction since the electric vector, which is parallel to the grain's long axis, suffers greater extinction than if it were perpendicular to it as shown in Figure 1.2.

Now if a group of non-spherical grains were randomly oriented in a region of space, and were illuminated by natural light, then one would not expect a net polarization to result since the superposition of the individual waves would tend to randomize their electric vectors. However, Hiltner (1951) showed that observations of solar type stars do in fact show polarization. Since solar type stars have very little dust in their immediate vicinity, (such as a circumstellar disk), and their net intrinsic polarization is extremely small, (Clarke et al. 1998), the most probable and widely accepted explanation for the origin of the observed polarization is due to aspherical dust grains which have a net, statistical alignment of their long axes in a preferred direction in the interstellar medium. Furthermore, observations of polarization of starlight have shown that the polarization vectors, when projected onto the plane of the sky, show a strong correlation with the galactic magnetic field (measured by Faraday rotation or the Zeeman effect for example) as well as a correlation with the reddening of stars. Therefore, there must exist a mechanism by which non-spherical dust grains can be aligned such that selective extinction creates polarization of the electric vectors predominately in the direction of the galactic magnetic field.

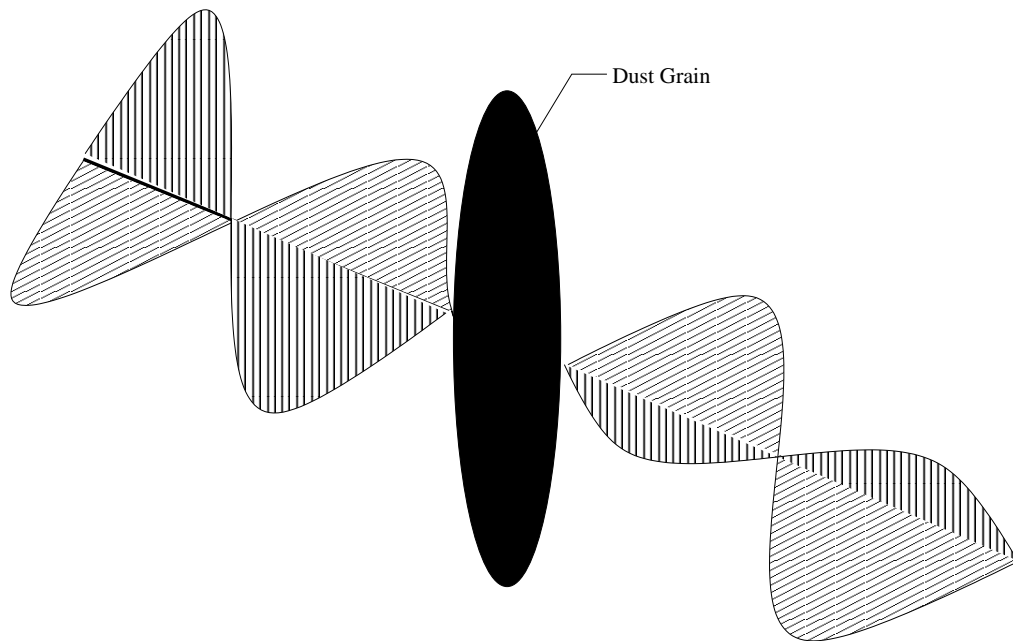


**Figure 1.2** Selective extinction of a dust grain. The electric vector suffers greater extinction when it is parallel to the long axis of the grain than when perpendicular.

This can be accomplished if the aspherical grains are spinning with their long axis perpendicular to the galactic magnetic field. By selective extinction then, the light will be partially polarized with the electric vector perpendicular to the long axes and hence parallel to the galactic magnetic field. The best explanation put forth by Davis and Greenstein (1951), hereafter DG, explains the alignment of dust grain by paramagnetic relaxation. While this explanation may have certain shortcomings, it is nonetheless regarded as the most likely way in which non-spherical grains become aligned with the magnetic field. While the entire derivation by DG will not be presented, we will present enough of their argument so that it may be seen how this method works. What follows is a brief explanation summarized from the original argument by DG.

Consider an aspherical dust grain which contains paramagnetic atoms or ions in a magnetic field which varies sinusoidally. The magnetic field may be described by the equation

$$\mathbf{B} = B_o \cos(\omega t + \delta) \quad (1.35)$$

where  $B_o$  represents the direction and amplitude of the magnetic oscillation. The magnetization of the paramagnetic material quoted by DG is then given by

$$\mathbf{M} = B_o[\chi' \cos(\omega t + \delta) + \chi'' \sin(\omega t + \delta)] \quad (1.36)$$

where  $\chi'$  and  $\chi''$  are the real and imaginary parts of the complex susceptibility, respectively. Now let the magnetic field be static and the grain rotate with a constant angular velocity  $\omega$  about an axis fixed in space and in the grain. Let the axes fixed in the grain be denoted by the unit vectors  $\mathbf{i}$ ,  $\mathbf{j}$ , and  $\mathbf{k}$  and the axes fixed in space by the unit vectors  $\hat{\mathbf{e}}_x$ ,  $\hat{\mathbf{e}}_y$ , and  $\hat{\mathbf{e}}_z$  both having a common origin. Also let the  $\mathbf{k}$  and  $\hat{\mathbf{e}}_z$  axes be collinear and let  $\omega$  be in this direction as well. At time  $t = 0$  all like axes coincide and the coordinate transformation is given by

$$\hat{\mathbf{e}}_x = \mathbf{i} \cos \omega t - \mathbf{j} \sin \omega t \quad (1.37)$$

$$\hat{\mathbf{e}}_y = \mathbf{i} \sin \omega t + \mathbf{j} \cos \omega t \quad (1.38)$$

$$\hat{\mathbf{e}}_z = \mathbf{k} = \frac{\omega}{\omega} \quad (1.39)$$

Now let the magnetic field in the fixed coordinate system be given by the following expression

$$\mathbf{B} = B_x \hat{\mathbf{e}}_x + B_z \hat{\mathbf{e}}_z \quad (1.40)$$

as shown in Figure 1.3. By using equations (1.37) – (1.39), this magnetic field can be written in terms of the rotating coordinate system as

$$\mathbf{B} = B_z \mathbf{k} + B_x \cos \omega t \mathbf{i} + B_x \cos\left(\omega t + \frac{\pi}{2}\right) \mathbf{j}. \quad (1.41)$$

From the point of view of the grain, there is a total magnetic field which is a superposition of the three fields: one static and two others which vary sinusoidally. Therefore, using equation (1.41) in equation (1.36) we see that the magnetization of the material has three components given by

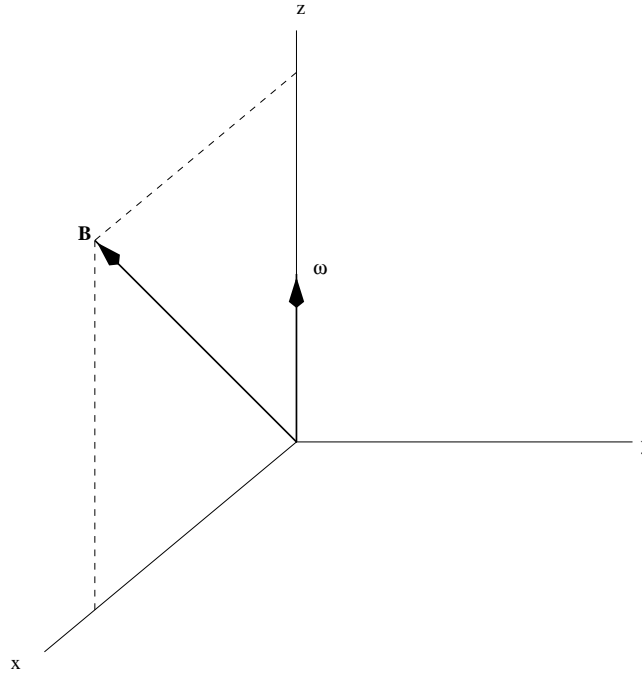


**Figure 1.3** Magnetic field direction relative to angular velocity of a rotating dust grain.

$$\mathbf{M}_x = B_x(\chi' \cos \omega t + \chi'' \sin \omega t) \mathbf{i} \quad (1.42)$$

$$\mathbf{M}_y = B_x(-\chi' \sin \omega t + \chi'' \cos \omega t) \mathbf{j} \quad (1.43)$$

$$\mathbf{M}_z = \chi_o B_z \mathbf{k} \quad (1.44)$$

where we have used the fact that if  $\omega = 0$ , then  $\chi'' = 0$  and  $\chi' = \chi_o$  the ordinary static susceptibility. Using the principle of superposition, the total magnetization can be written as

$$\mathbf{M} = B_x[(\chi' \cos \omega t + \chi'' \sin \omega t) \mathbf{i} + (-\chi' \sin \omega t + \chi'' \cos \omega t) \mathbf{j}] + \chi_o B_z \mathbf{k} \quad (1.45)$$

Since both  $\mathbf{B}$  and  $\mathbf{M}$  are non-zero, and are not collinear, there will exist a torque on the grain due to the magnetization of the paramagnetic material. The torque due to a magnetic moment  $\mathbf{m}$  is expressed by the equation  $\boldsymbol{\tau} = \mathbf{m} \times \mathbf{B}$ . If the grain has a volume  $V$ , then the magnetic moment is  $V\mathbf{M}$  and the torque equation becomes  $\boldsymbol{\tau} = V\mathbf{M} \times \mathbf{B}$ . Therefore, the torque on the grain is found by using this equation with  $\mathbf{M}$  and  $\mathbf{B}$  given by equations (1.45) and (1.41) respectively

$$\boldsymbol{\tau} = V\mathbf{M} \times \mathbf{B} = (\chi_o - \chi')B_z B_x \hat{\mathbf{e}}_y + V\chi''[-B_x^2 \hat{\mathbf{e}}_z + B_x B_z \hat{\mathbf{e}}_x] \quad (1.46)$$

or in terms of  $\boldsymbol{\omega}$  and  $\mathbf{B}$

$$\boldsymbol{\tau} = V(\chi_o - \chi')\boldsymbol{\omega}^{-2}(\boldsymbol{\omega} \cdot \mathbf{B})(\boldsymbol{\omega} \times \mathbf{B}) + V\chi''\boldsymbol{\omega}^{-1}(\boldsymbol{\omega} \times \mathbf{B}) \times \mathbf{B} \quad (1.47)$$

According to DG, since the first term is perpendicular to  $\boldsymbol{\omega}$ , it does not affect the rotational kinetic energy, but produces a precession and has no significant effect on the orientation. It is the second term which is important to the motion of the grain. The manner in which this torque affects the grains motion can be seen in Figure 1.4 below.

In this figure,  $\mathbf{L}$  is the angular momentum vector which is fixed in space. The grain is spinning about the axis of symmetry  $OA$  which is nutating about  $\mathbf{L}$  and the angular velocity  $\boldsymbol{\omega}$  is obtained by the sum of the rotations about  $\mathbf{L}$  and  $OA$ . Therefore,  $\boldsymbol{\omega}$  moves relative to both space and the grain, but always in the plane formed by  $\mathbf{L}$  and  $OA$ . The equations of motion derived by Davis and Greenstein which describe the rate of change of angular momentum and rotational kinetic energy are

$$\frac{d\mathbf{L}}{dt} = V\chi''\boldsymbol{\omega}^{-1}(\boldsymbol{\omega} \times \mathbf{B}) \times \mathbf{B} \quad (1.48)$$

$$\frac{dK_r}{dt} = \boldsymbol{\tau} \cdot \boldsymbol{\omega} = -V\chi''\boldsymbol{\omega}^{-1}(\boldsymbol{\omega} \times \mathbf{B})^2 \quad (1.49)$$

where  $K_r$  is the rotational kinetic energy, and equation (1.48) is simply a restatement of equation (1.47) using  $d\mathbf{L}/dt = \boldsymbol{\tau}$  and the first term ignored. Now when the first equation is averaged over a single nutation, the average angular velocity  $\boldsymbol{\omega}_{av}$  will be parallel to  $\mathbf{L}$  and  $\boldsymbol{\tau}_{av}$  will be normal to  $\mathbf{B}$  and lie in the plane of  $\mathbf{L}$  and  $\mathbf{B}$  as shown in Figure 1.4.

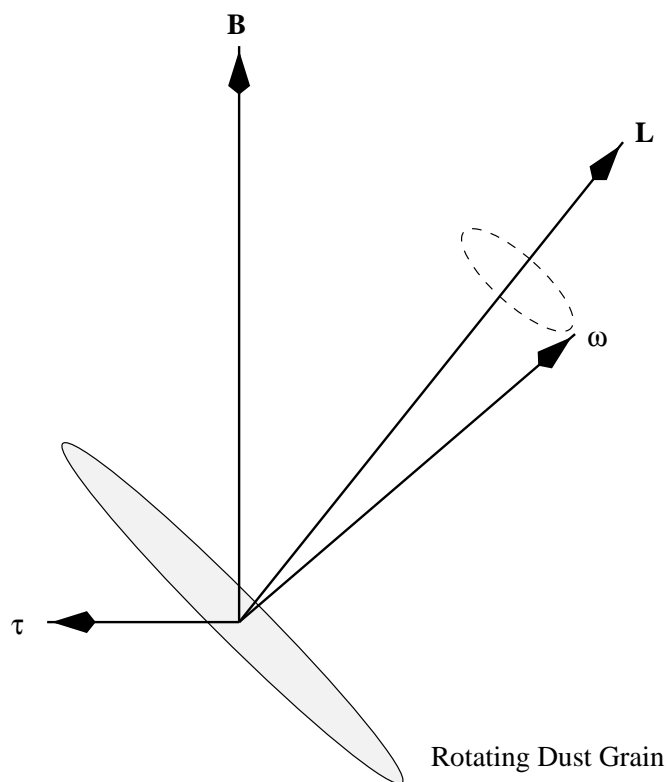


**Figure 1.4** Average torque on a grain rotating with angular velocity  $\omega$  in a magnetic field.

Therefore, according to equation (1.48),  $\mathbf{L}$  will approach  $\mathbf{B}$  in such a manner as to keep constant the component of  $\mathbf{L}$  along  $\mathbf{B}$ . Since the right hand side of equation (1.49) is negative, the kinetic energy of rotation will decrease until  $\omega$  is parallel to  $\mathbf{B}$ . In order for the above to occur, the grain must rotate about its shortest axis. Thus, the eventual state of the grain, due to the acting torque, is one where the grain is spinning about its shortest axis with that axis being parallel to  $\mathbf{B}$ .

While this has been a quick summary of the argument of paramagnetic relaxation presented by Davis and Greenstein (1951) and many other calculations have been omitted, it shows the salient features of the model. While this model explains how grains can be aligned with a magnetic field, it does have its shortcomings. Purcell and Spitzer (1971) and Aannestad and Purcell (1973) have shown that, for specific grain models, the minimum required magnetic field needed for alignment is on the order of  $10^{-9}$  T, whereas, in the solar neighborhood, measurements of the magnetic field by Zeeman splitting and Faraday rotation indicate an average value on the order of  $10^{-10}$  T. Another objection is that in dense molecular clouds a high degree of polarization is usually observed, but should not occur. The reason for this is that since the gas is denser in these regions, there will be more collisions with the grain which will tend to randomize the motion of the grain. Therefore, if collisional thermal equilibrium is reached between the gas and the grains, then the Davis-Greenstein mechanism fails. However, while other models have been proposed, they all share in common the fact that non-spherical grains are aligned with the galactic magnetic field and this is the reason interstellar polarization occurs.

### 1.3 Expected Results

The focus of this thesis is the acquisition of data concerning the linear polarization of  $H\alpha$  light from shell structures and supernova remnants. The technique used employs a rotating polarizer placed in front of a narrow bandpass  $H\alpha$  interference filter with images obtained using a cryogenically cooled CCD camera. A rotating polarizer device was designed, built, and used in conjunction with the Spectral Line Imaging Camera (SLIC) at Virginia Tech's Martin Observatory in Giles County, Virginia. The SLIC records a usable  $10^\circ$  diameter

field-of-view of faint extended galactic  $H\alpha$  emission. Using the rotating polarizer device with the SLIC, I was able to create polarization maps over a  $10^\circ$  diameter region along selected areas in the galactic plane.

Stars are ubiquitous in the images from the SLIC. While the camera was designed to be insensitive to stars, I nonetheless tried to detect interstellar polarization of starlight due to selective extinction by elongated dust grains. This was rather difficult since the degree of interstellar polarization of starlight is typically on the order of 1% or less. A positive detection of polarization for stars was also used as a diagnostic to not only measure the ability of the camera to accurately detect polarization but also to provide a means of determining the alignment accuracy of the rotating polarizer device. A positive detection also allowed me to place limits on the degree of polarization which can be detected using this method.

As mentioned in this introduction, polarization of starlight results from selective extinction by elongated dust grains aligned with the galactic magnetic field. By mapping the projection of polarization vectors on the plane of the sky we can learn about the direction of the galactic magnetic field, particularly as it relates to shell like structures. I imaged shell structures and supernova remnants in the constellations of Cygnus and Monoceros, (which were seen in the  $H\alpha$  images of the SLIC during the galactic survey), with the hope that polarization vectors from stars around the periphery of these structures would yield information about the magnetic fields associated with them.

Since the SLIC was designed to detect  $H\alpha$  emission, I naturally took advantage of this. Just as the light from stars is thermal in origin and most lack intrinsic polarization,  $H\alpha$  emission from HII regions lack intrinsic polarization as well. Therefore, similar to the detection of interstellar polarization using starlight, I tried to detect interstellar polarization using  $H\alpha$  emission from HII regions. While the possible information provided by stellar polarization around these objects can occur only at discrete locations, the use of  $H\alpha$  emission over the entire nebula may provide a more continuous distribution of polarization information. Detecting polarization by selective extinction using  $H\alpha$  light coupled with a rotating polarizer is a unique way to map the distribution of polarization over extended emission regions.

I expected some polarization by scattering to be observed since scattered light is prevalent throughout the ISM. While the degree of polarization around reflection nebulae can be quite high ( up to  $\sim 70\%$  in certain nebulae ), the size of such regions is typically small compared to the field-of-view offered by the SLIC. I did not image any specific reflection nebulae. However, scattering by dust will be examined around HII regions, since it was detected. The original goal of this project was to detect polarization by selective extinction due to elongated dust grains aligned with structured magnetic fields. While results from selective extinction were few, polarization by scattering by grains surrounding the HII region NGC 2237-9 (the Rosette Nebula) turned out to be very important.